Comparison of Proton Irradiation Effects on Electrical Properties of Quasi-Vertical and Lateral GaN Schottky Barrier Diodes

Yun Tang, Xintian Zhou, Boya Zhang, Mingwei Li, Yunpeng Jia, Dongqing Hu, Yu Wu, *Member, IEEE*, Lihao Wang, Bodian Li, Xuanwu Kang, Lei Wang, and Yuanfu Zhao

***Abstract*— In this article, quasi-vertical and lateral gallium nitride (GaN) Schottky barrier diodes (SBDs) with similar electrical parameters are irradiated with 200-keV protons at different fluences. The radiation-induced defects induced by irradiation affect carrier concentration and tunneling current, result in a slight decrease in the forward current and an increase in the reverse current of quasi-vertical GaN SBDs. In contrast, lateral GaN SBDs exhibit significant degradation in forward current characteristics and a reduction in reverse current postirradiation. Electrical parameter variations in the N^--GaN and N^+-GaN layers of quasi-vertical SBDs, as well as changes in 2-D electron gas (2DEG) concentration at the AlGaN/GaN heterojunction interface in lateral diodes, are analyzed through C–V, transmission line model (TLM), and Hall measurement. By combining stopping and range of Ions in matter (SRIM) and technology computer-aided design (TCAD) simulations, the types and distributions of radiation-induced defects in both GaN SBDs are modeled to comprehensively reveal the degradation mechanisms in both devices under proton irradiation.**

***Index Terms*— Gallium nitride (GaN), lateral Schottky barrier diode (SBD), proton irradiation, quasi-vertical SBD.**

I. Introduction

GaN has excellent material properties, such as high breakdown electric field, high mobility, and high-electron-saturation drift velocity, so that it is considered the most potential candidate material for high power and voltage electronic devices [1], [2].

Gallium nitride (GaN) Schottky barrier diodes (SBDs) have been gradually applied in switching and discrete limiter modules in recent years due to their high-power capacity at high frequency [3], [4]. Two common structures of GaN SBDs, namely quasi-vertical and lateral, exhibit distinct characteristics in terms of conduction mechanisms and device geometry [5], [6], [7], [8], [9].

Received 12 December 2024; accepted 14 December 2024. Date of publication 19 December 2024; date of current version 21 January 2025. This work was supported by the National Natural Science Foundation of China under Grant 62204011. *(Corresponding authors: Xintian Zhou; Yunpeng Jia.)*

Yun Tang, Xintian Zhou, Boya Zhang, Mingwei Li, Yunpeng Jia, Dongqing Hu, and Yu Wu are with the School of Information Science and Technology, Beijing University of Technology, Beijing 100124, China (e-mail: 18810371895@139.com; jyp@bjut.edu.cn).

Lihao Wang is with Beijing Microelectronics Technology Institute, Beijing 100076, China.

Bodian Li is with the Network Science Institute, Northeastern University, Boston, MA 02115 USA.

Xuanwu Kang and Lei Wang are with the Institute of Microelectronics, Chinese Academy of Sciences, Beijing 100029, China (e-mail: kangxuanwu@ime.ac.cn; wangle@ime.ac.cn).

Yuanfu Zhao is with the Faculty of Information Technology, Beijing University of Technology, Beijing 100124, China, and also with Beijing Microelectronics Technology Institute, Beijing 100076, China.

Color versions of one or more figures in this article are available at https://doi.org/10.1109/TNS.2024.3520476.

Digital Object Identifier 10.1109/TNS.2024.3520476

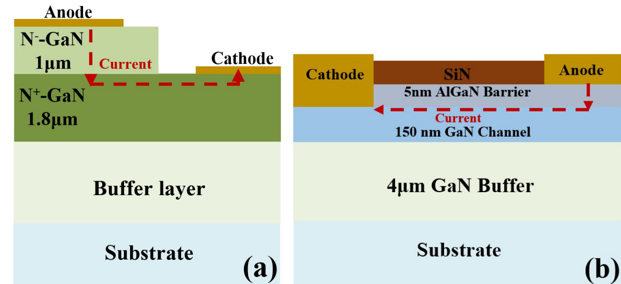

Fig. 1. Schematic cross section of epitaxial structure of (a) quasi-vertical GaN SBDs and (b) lateral GaN SBDs.

The quasi-vertical GaN SBD, as shown in Fig. 1(a), exhibits a peak electric field located in the drift layer with a more uniform distribution, which contributes to excellent blocking characteristics. By simply increasing the thickness of the N^--GaN drift layer, the breakdown voltage can be enhanced, allowing for a smaller device area and higher integration density. However, its conduction and blocking characteristics are influenced by the doping concentration of the drift layer, necessitating a design tradeoff for optimized performance. Additionally, deep etching processes involved in its fabrication may introduce more defects in the device, leading to a reduction in device reliability.

On the other hand, as shown in Fig. 1(b), lateral GaN SBDs conduct current primarily between the AlGaN and GaN layers, relying on spontaneous and piezoelectric polarization effects [10], [11]. When the Al composition in AlGaN is between 0.2 and 0.3, a significant density of polarization-induced positive charges accumulates at the heterojunction interface. To maintain electrical neutrality, free electrons are induced on the GaN side of the interface. These electrons are attracted by the high-density positive charges near the heterojunction, forming a narrow and deep quantum well, confining the electrons and creating a highly concentrated 2-D electron gas (2DEG) at the interface. The high concentration of 2DEG ensures excellent conduction properties, while the undoped GaN channel layer enables high electron mobility. Sharing the

0018-9499 © 2024 IEEE. All rights reserved, including rights for text and data mining, and training of artificial intelligence and similar technologies. Personal use is permitted, but republication/redistribution requires IEEE permission. See https://www.ieee.org/publications/rights/index.html for more information.

epitaxial layer structure with high-electron-mobility transistors further facilitates integration in module applications. However, lateral AlGaN/GaN SBDs exhibit a higher electric field concentration at the surface, which can increase reverse leakage current due to localized field effects. The lower barrier on the GaN side allows carriers in the channel to spill over, weakening 2DEG confinement and resulting in device performance degradation. Additionally, increasing the breakdown voltage of lateral diodes requires proportional increases in the distance between the anode and the cathode, leading to larger device dimensions and associated manufacturing costs.

It has been reported that GaN device operation in harsh radiation environments, such as those encountered in space or nuclear applications, presents significant challenges [12], [13], [14], [15], [16], [17], [18], [19], [20]. Given that both types of GaN SBDs are used in similar application scenarios, it is essential to understand and compare the performance degradation of different GaN SBDs under irradiation to ensure the reliability and robustness of electronic systems in such environments. Due to the wide bandgap and high-ionization-energy characteristics of GaN materials, GaN diodes theoretically have superior tolerance to radiation damage in radiation environments. In [18], N-GaN SBDs were irradiated by a ^{60}Co gamma ray. After a cumulative irradiation dose of 21 Mrad(Si), the reverse leakage current increased slightly, whereas the forward current was almost unchanged. However, GaN diodes are more sensitive to the displacement effect. In [19], 1-MeV proton irradiation increases the ideality factor and series resistance on the N-GaN SBDs. In [20], the carrier removal effect in the lateral AlGaN/GaN SBD irradiated by 3-MeV protons is predominantly influenced by bulk traps in the AlGaN layer. Despite the extensive research on the radiation effects in GaN SBDs, most studies focus separately on lateral and vertical structures. Variations in device epitaxial structure (substrate and buffer layers), electrical parameters, as well as irradiation particle type and energy all influence the analysis of performance degradation mechanisms under irradiation for the two different GaN SBD structures.

In this article, the radiation tolerance of quasi-vertical and lateral GaN SBDs, which have similar electrical parameters, is compared. Considering that GaN SBDs exhibit higher sensitivity to displacement damage compared to ionizing radiation, the 200-keV proton irradiation effects on both GaN SBDs are investigated. Through current–voltage $(I–V)$, capacitance–voltage $(C–V)$, transmission line model (TLM), Hall measurements, and technology computer-aided design (TCAD) simulation, degradation mechanisms of lateral and quasi-vertical GaN SBDs are revealed in detail.

II. Experimental Details

Fig. 1 shows the schematic cross section of the quasi-vertical and lateral GaN SBDs. Both epitaxies are grown on C plane sapphire substrates by metal-organic chemical vapor deposition (MOCVD). For quasi-vertical GaN SBDs, a 2-μm buffer layer was grown first, followed by 3-μm N$^+$-GaN (Si: 5×10^{18} cm^{-3}) and 1-μm high-quality N$^-$-GaN (Si: $<1 \times 10^{16}$ cm^{-3}) drift layers. For lateral GaN SBDs, a 4-μm GaN buffer layer was grown first, followed by a

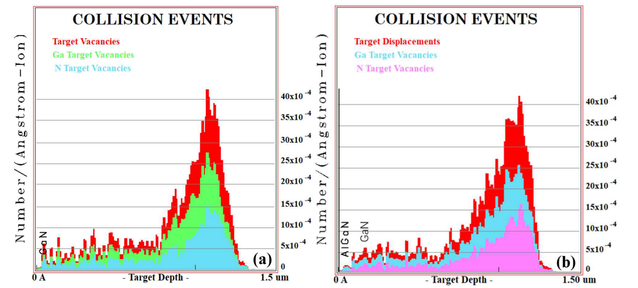

Fig. 2. SRIM simulation defects distribution of 200-keV protons in (a) quasi-vertical and (b) lateral GaN SBDs.

150-nm undoped GaN channel layer and a 5-nm AlGaN barrier layer. The SiN passivation layer was deposited by low-pressure chemical vapor deposition (LPCVD) with a thickness of about 20 nm and followed by plasma-enhanced chemical vapor deposition (PECVD) with a thickness of 180 nm. The space between the anode and the cathode is 2 μm. The cathode ohmic metal stack Ti/Al/Ni/Au and anode Schottky metal stack Ni/Au were deposited for both GaN SBDs.

Devices under tests (DUTs) were irradiated by a 200-keV proton beam in a vacuum environment at room temperature in Harbin Institute of Technology. During the radiation, DUTs were biased at -20 V. The proton fluence was set as 1×10^{12} and 1×10^{13} p/cm^2. The Schottky contact diameter for both types of diodes is 150 μm. The breakdown voltage ($I = 100$ μA) of the quasi-vertical diode and lateral diode are 55 and 60 V, respectively.

Keysight B1505 Power Device Analyzer was used to take data in $I–V$ and $C–V$ measurements at room temperature, and the latter measurement was carried out at the frequency of 1 MHz. HMS-5300 Hall equipment was used to measure carrier concentration and mobility. In all cases, electrical measurements were taken 24 h after the proton irradiation.

III. Experimental Results and Discussion

A. Proton Projection Range Simulation

The defect distribution resulting from 200-keV proton irradiation in quasi-vertical and lateral GaN SBDs was simulated using stopping and range of Ions in matter (SRIM) software. A total of 1×10^3 protons were simulated. As shown in Fig. 2, the proton penetration depth is 1.4 μm, with the defect peak occurring at 1.1 μm. This defect peak corresponds to a position of 0.1 μm in the N$^+$-GaN layer of quasi-vertical diodes and 0.9 μm in the buffer layer of lateral diodes.

B. Electrical Characteristics of Quasi-Vertical GaN SBDs Under Proton Irradiation

Fig. 3 shows forward and reverse characteristics of quasi-vertical GaN SBDs at 300 K. It can be observed that the forward current of the SBD degrades slightly, while the reverse current shows a more noticeable increase as the proton fluence increases. Fig. 4(a) and (b) shows the schematic of current flow under forward and reverse biases for quasi-vertical GaN SBDs. In the case of forward bias, the barrier on the GaN side decreases, leading to an increased number

TABLE I

CALCULATED $N_D - N_A$ CONCENTRATION IN THE N^--GAN LAYER OF QUASI-VERTICAL SBDS UNDER DIFFERENT FLUENCE

Fluence (p/cm^2)	Original	1×10^{12}	1×10^{13}
N_D-N_A (cm^{-3})	5.0×10^{15}	5.0×10^{15}	4.4×10^{15}

TABLE II

R_{SH}, CARRIER CONCENTRATION, AND MOBILITY OF THE N^+-GAN LAYER FOR QUASI-VERTICAL SBDS UNDER VARIOUS PROTON FLUENCES

fluence (p/cm^2)	Original	1×10^{12}	1×10^{13}
R_{SH}(Ω/□)	0.17	0.17	0.17
Carrier concentration (cm^{-3})	1.02×10^{18}	1.04×10^{18}	1.02×10^{18}
Mobility (cm^2·V^{-1}·s^{-1})	486	490	487

of electrons moving from GaN to the metal and forming a forward current. Thermionic emission is the primary current transport mechanism in SBDs, which is predominantly composed of majority carriers in the N^--GaN layer. Through the C–V measurements, the variation of carrier concentration in the N^--GaN layer after proton irradiation can be obtained. Fig. 5(a) shows $1/C^2$ versus reverse voltage for GaN SBDs at room temperature, and $N_D - N_A$ of the N^--GaN drift layer can be extracted by

$$\frac{d(1/C^2)}{dV} = \frac{2}{qA^2\varepsilon\varepsilon_S(N_D - N_A)} \tag{1}$$

where N_D and N_A are the donor and acceptor doping concentrations, respectively. ε_s is the permittivity of GaN. The calculated $N_D - N_A$ of the N^--GaN layer is shown in Table I, indicating a decrease in $N_D - N_A$ at the fluence of 1×10^{13} p/cm^2. As the electron concentration in the N^--GaN layer decreases after irradiation, the forward current of the device correspondingly decreases.

In addition, the degradation in the electrical performance and ohmic contact of the N^+-GaN layer under various irradiation fluences can be evaluated through the TLM and Hall measurements. Fig. 5(b) illustrates the I–V curves of the N^+-GaN TLM samples. R_{SH} can be extracted by the following equation:

$$R_{\text{total}} = \frac{R_{SH}}{2\pi}\left[\ln\left(\frac{r_n}{r_0}\right) + L_T\left(\frac{1}{r_n} + \frac{1}{r_0}\right)\right] \tag{2}$$

where L_T is the transfer length, and r_0 and r_n represent the radii of the inner and outer rings of the TLM structure, respectively. The measured R_{SH}, carrier concentration, and mobility of N^+-GaN are shown in Table II. It can be observed that N^+-GaN exhibits almost no performance degradation under proton irradiation, although the defects induced by the proton irradiation are primarily localized within the N^+-GaN layer.

When the SBDs under reverse bias, electrons overcome the barrier and enter the semiconductor from metal, resulting in the generation of reverse leakage current. The main leakage current mechanism is thermionic emission while tunneling currents also contribute to the formation of reverse current. Using TCAD simulations, the variations in the reverse current of quasi-vertical SBDs before and after irradiation are modeled. For the simulation modeling of

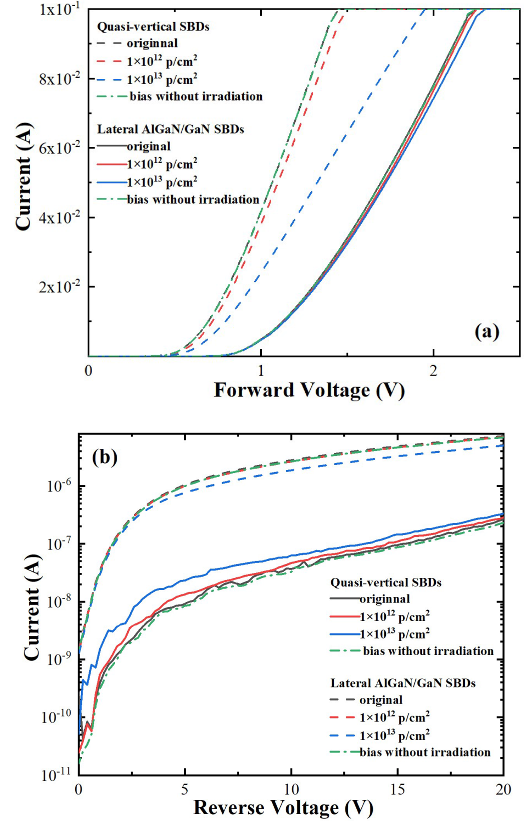

Fig. 3. I–V characteristic curves of quasi-vertical GaN SBDs under different proton irradiation fluence. (a) Forward bias I–V characteristics. (b) Reverse bias I–V characteristics. Green curves illustrate SBDs subjected to a −20-V bias without irradiation, having the same stress time as those exposed to a fluence of 1×10^{13} cm^2.

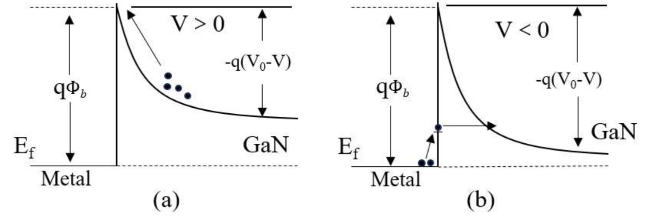

Fig. 4. Schematic of the (a) current flow under forward voltage and (b) TAT under reverse bias for quasi-vertical GaN SBDs.

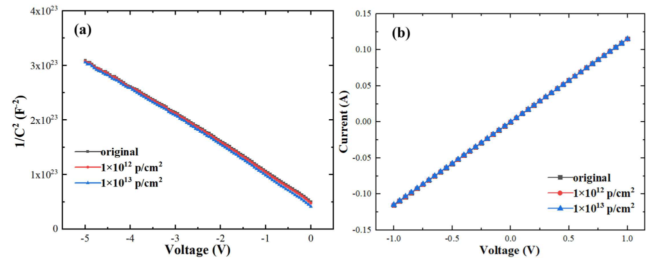

Fig. 5. (a) Measured $1/C^2$ versus reverse voltage for SBDs. (b) I–V curves of the N^+-GaN TLM sample under various proton fluences.

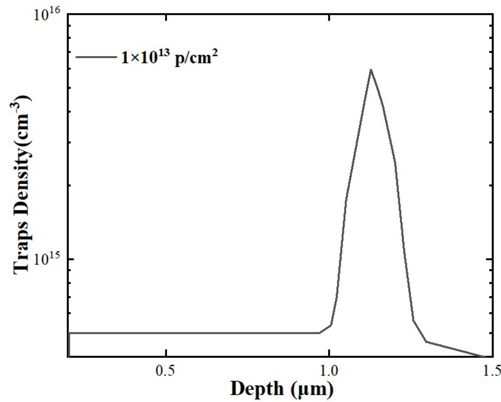

Fig. 6. Trap density distribution along the proton incident depth in the GaN layer.

quasi-vertical GaN SBDs, appropriate physical models are employed to ensure accuracy and reliability. These include compound models (Schockley–Read–Hal (SRH), Avalanche), mobility models (HighFieldSaturation, DopingDependence), polarization, anisotropic Poisson models, Fermi–Dirac and Schockley–Read–Hall statistics. The defect density distribution in the GaN layer induced by irradiation can be obtained by multiplying the number of defects generated along the proton irradiation path, as determined by SRIM simulation, by the proton fluence. To simulate the distribution of traps generated by proton irradiation in TCAD software, traps following a Gaussian distribution are incorporated at a depth of 0.1 μm in the N^+-GaN layer. Additionally, constant doping profiles are applied to the GaN layers along the path of proton irradiation (as shown in Fig. 6). Based on the calculation, the peak defect density generated in the N^+-GaN layer is 4×10^{15} cm^{-3} under a fluence of 1×10^{13} p/cm^2.

It has been reported that low-energy proton irradiation introduces various traps in the GaN layer, including a trap at E_C-0.2 eV, a donor-like trap at E_C-0.8 eV, and an acceptor-like trap at E_C-0.6 eV [21]. The trap at E_C-0.2 eV is commonly attributed to donor defects such as nitrogen vacancies (V_N) and the dehydrogenation of passivated substitutional oxygen impurities (O_N–H) [22], [23]. The acceptor-like trap at E_C-0.6 eV is associated with iron impurity (Fe_{Ga}), which is a common substitutional impurity in the GaN buffer layer [24], [25], [26], [27]. Irradiation induces the dehydrogenation of Fe_{Ga}–H in the buffer layer. As for the trap at E_C-0.8 eV, while some reports attribute it to gallium interstitial, its high formation energy and absence in recent device studies suggest that it may have been introduced due to immaturity in early GaN epitaxial growth [28], [29]. Therefore, the trap at E_C-0.8 eV will not be further considered in this discussion. In addition, the gallium vacancy (V_{Ga}) at E_C-2 eV exhibits a low formation energy as an acceptor defect in N-type GaN. After proton irradiation, V_{Ga} is generated in the GaN layer [22], [30].

For quasi-vertical GaN diodes, the proton penetration depth is approximately 1.4 μm, which does not extend into the buffer layer. Consequently, irradiation-induced dehydrogenation of Fe_{Ga}-H is negligible. Therefore, acceptor defects in simulations are V_{Ga}. Fig. 7(a) shows the electric field distribution for quasi-vertical SBDs. The electric field is predominantly

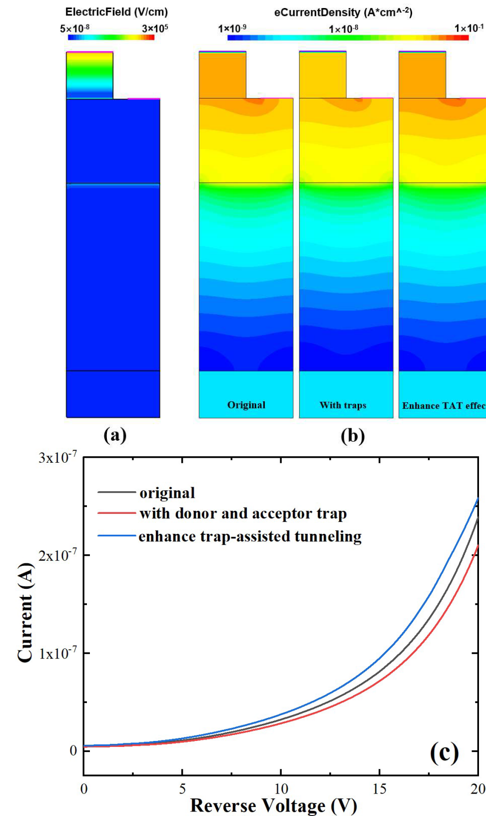

Fig. 7. (a) Electric field distribution of quasi-vertical SBDs under −20 V. (b) Electron current density distribution and (c) reverse current curves of quasi-vertical SBDs with and without various traps, along with the reverse current curve of the SBD after enhancement in TAT tunneling.

located at the N^--GaN layer of the device. In Fig. 7(b) and (c), it can be observed that, compared to the original device, the reverse current of the device with introduced donor- and acceptor-like traps decreases slightly. SRIM simulations indicate that irradiation generates a higher density of V_{Ga} than V_N in the N-GaN layer, suggesting that acceptor-like defects have a more significant impact on the device. Acceptor-like defects capture electrons, leading to a reduction in the reverse current. The peak acceptor-like defects concentration is calculated to be 2.5×10^{15} cm^{-3}, while the doping concentration of the N^+-GaN layer at the peak is 5×10^{18} cm^{-3}, implying that the compensating effect of acceptor defects in the N^+-GaN region is negligible. In the N^--GaN layer, where the doping concentration is relatively lower, the compensating effect of acceptor-like defects becomes slightly more significant, consistent with previous C–V and Hall measurements. Previous studies have reported that V_N at the metal/GaN interface can enhance trap-assisted tunneling (TAT) [31]. Based on the device with introduced traps, the TAT effect is further enhanced, leading to an increase in reverse current, which aligns with experimental results. Hence, it can be concluded that the increase in reverse current in quasi-vertical GaN SBD is caused by the irradiation-induced V_N defects at the metal/GaN interface, which increase the tunneling current.

C. Electrical Characteristics of Lateral AlGaN/GaN SBDs Under Proton Irradiation

Fig. 3(a) shows the forward I–V characteristics of lateral SBDs at 300 K. Different from quasi-vertical SBD, the forward

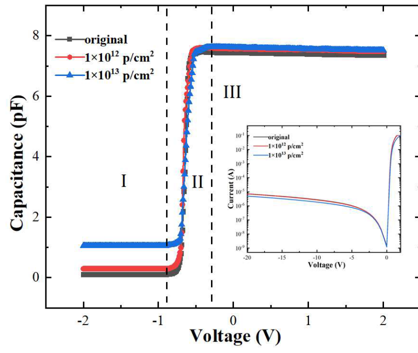

Fig. 8. C–V curves for lateral SBDs under various proton irradiation fluence. The inset shows the full scale of the I–V curve for lateral AlGaN/GaN SBDs.

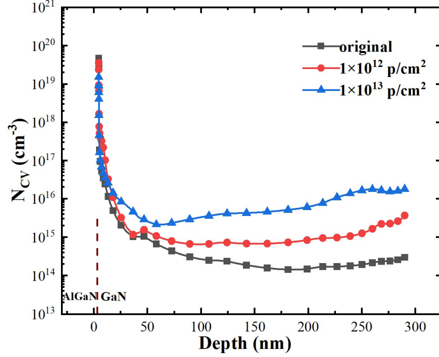

Fig. 9. Carrier concentration N_{cv} distribution as a function of depth under various proton fluences.

current of lateral SBDs degrades significantly as the proton fluence increases. The C–V curves of the lateral SBDs under various proton fluences are shown in Fig. 8. Based on the data in Fig. 8, Fig. 9 illustrates the detailed carrier concentration distribution along the depth. The C–V curves can be divided into three parts. Part I reflects the carrier concentration in the GaN channel and the buffer layer when the 2DEG is depleted under the reverse voltage. Part II is the process of 2DEG transformation from depletion to accumulation. In Part III, electrons accumulated in the AlGaN layer under the forward bias, which represents the accumulation part of the C–V curves.

As the irradiation fluence increases, the capacitance in part III of the C–V curve increases, indicating an increase in the number of trapped electrons in the AlGaN layer. Under an applied forward voltage, more electrons are trapped as the 2DEG crosses the AlGaN layer. This defect should be attributed to the O_N undergoing a "DX-like" reconfiguration, exhibiting acceptor-like behavior in the AlGaN layer [22], [32], [33]. Acceptor-like defects exhibit electronegativity upon capturing electrons, leading to an increase in capacitance. Additionally, the capacitance in part I of the C–V curves significantly increases with rising fluences, attributed to the formation of acceptor defects in the GaN channel and buffer layers. As shown in Fig. 8, the 2DEG concentration in the AlGaN/GaN channel decreases after irradiation, with the increase of trapped electrons in the GaN channel and buffer layers. Due to the thinness of the AlGaN layer (5 nm), it is hard to directly calculate the trapped electron concentration in the AlGaN layer with the equipment limitations. The electron trapping in the AlGaN layer after proton irradiation

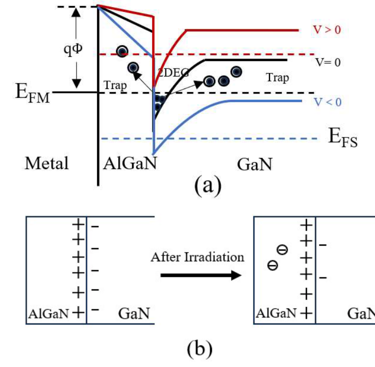

Fig. 10. (a) Schematic band diagram for lateral AlGaN/GaN SBDs under various bias voltages. (b) Variation of polarized charge on the AlGaN/GaN interface before and after irradiation.

has been confirmed in [20]. The schematic illustrating electron trapping in the AlGaN and GaN layers is shown in Fig. 10(a). As depicted in Fig. 10(b), an increase in negatively charged defects in the AlGaN layer induces an opposing polarization field at the AlGaN/GaN interface, which reduces the polarization intensity of the heterojunction interface and further diminishes the 2DEG concentration [34]. This reduction in 2DEG concentration consequently decreases the forward current of the lateral SBD. This phenomenon, in which proton irradiation-induced acceptor defects capture electrons, leading to a decrease in output current, also appears in GaN HEMT devices [35], [36].

Unlike quasi-vertical diodes, protons can penetrate the buffer layer of lateral diodes. Consequently, in simulations, the radiation-induced acceptor defect level in the GaN channel layer is set to E_C-2 eV, while acceptor defects in the buffer layer are E_C-2 eV and E_C-0.6 eV. Fig. 11(a) presents the simulated distribution of electron current density. When the lateral SBD is in conduction, electrons in the channel not only move along the AlGaN/GaN interface but also extend into the AlGaN layer, the GaN channel layer, and the GaN buffer layer. Simulations on lateral SBDs with traps, as shown in Fig. 11(b), indicate that proton irradiation-induced acceptor defects have minimal effect on the forward current. This is likely due to the low defect density in the AlGaN and GaN channel layers, providing limited compensation for the 2DEG. When the polarization intensity at the heterojunction is reduced in simulations, a significant decline in forward current is observed, consistent with experimental results. Therefore, it can be concluded that the negatively charged defects in the AlGaN layer reduce the polarization intensity of the heterojunction, leading to a decrease in 2DEG concentration, which is the primary cause of forward current degradation in AlGaN/GaN SBDs after proton irradiation.

Fig. 3(b) shows reverse I–V characteristics of lateral GaN SBDs. It should be noted that the reverse leakage current of lateral GaN SBDs decreases with increasing irradiation fluence. In Fig. 12(a), there is a high peak electric field at the edge of the anode for lateral SBDs. Under the effect of the electric field, the 2DEG in the AlGaN/GaN channel near the anode is depleted. Electrons are injected from the anode into the GaN channel and the buffer layer under the

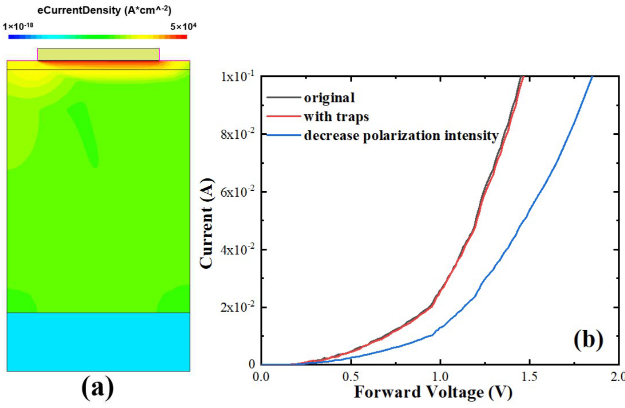

Fig. 11. (a) Distribution of electron current density in a lateral SBD under forward voltage and (b) forward current curves of lateral SBDs with and without various traps, along with the forward current curve of the lateral SBD after a reduction in polarization strength.

electric field, moving toward the cathode. Upon reaching the edge of the depletion region, electrons reenter the AlGaN/GaN channel and are eventually collected by the cathode. Unlike quasi-vertical diodes, due to the presence of the AlGaN layer, electrons are prevented from directly tunneling from the metal into the GaN, V_N in the GaN channel layer does not contribute to tunneling current formation. Instead, acceptor-like defects have a more significant influence on the device, leading to a reduction in reverse current. Fig. 13 shows the distribution of electron-trapped charge, clearly indicating that most of the electrons are trapped in the region below the cathode. Although the peak of irradiation-induced defects is in the GaN buffer layer, defects generated in the GaN channel layer near the 2DEG have a more significant impact on the reverse current.

D. Comparison of Proton Irradiation Effects on Quasi-Vertical and Lateral AlGaN/GaN SBDs

Due to the different structure and conduction mechanisms of quasi-vertical and lateral SBDs, the degradation degree of electrical characteristics is also different after proton irradiation. Table III is a summary of forward and reverse electrical characteristics for quasi-vertical and lateral SBDs with various proton fluences. The turn-on voltage (V_{on}) is extracted at $I =$ 1 mA and the reverse current (I_R) is measured at the reverse voltage of 20 V. The ideal factor n of diodes is calculated by fitting the linear region of forward current curves.

For the quasi-vertical GaN SBD, V_{on} remains consistent at 0.85 V before and after proton irradiation, only slightly decreasing to 0.87 V at a fluence of 1×10^{13} p/cm^2. I_R increases with higher irradiation fluence, rising from 2.6×10^{-7} to 3.5×10^{-7} A. Additionally, the ideal factor n shows minimal change, increasing slightly from 1.10 to 1.13 after irradiation. In contrast, the lateral GaN SBD exhibits more significant performance degradation. V_{on} increases progressively from 0.51 V before irradiation to 0.67 V. I_R, however, decreases as the irradiation fluence increases, dropping from 7.3×10^{-6} to 5.1×10^{-6} A. The ideality factor n also shows a marked increase from 1.23 to 1.51, indicating a greater impact of proton irradiation on its performance.

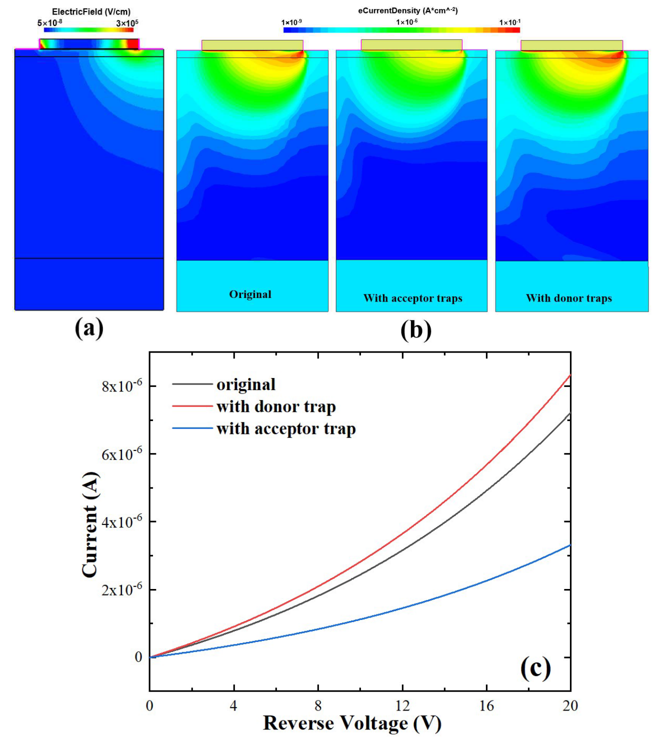

Fig. 12. (a) Electric field distribution of lateral SBDs under −20 V. (b) Electron current density distribution and (c) reverse current curves of lateral SBDs with and without various traps.

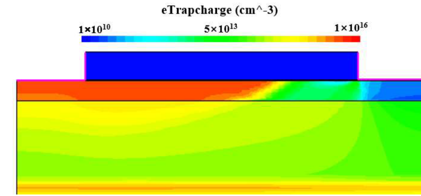

Fig. 13. Distribution of trapped electrons in the GaN layer with acceptor traps.

TABLE III

SUMMARY OF V_{on}, I_R, AND n FOR QUASI-VERTICAL AND LATERAL GaN SBDS UNDER VARIOUS PROTON FLUENCES

	fluence (p/cm^2)	Original	1×10^{12}	1×10^{13}
Quasi-vertical	V_{on} (V)	0.85	0.85	0.87
	I_R (A)	2.6×10^{-7}	2.8×10^{-7}	3.5×10^{-7}
	n	1.10	1.10	1.13
Lateral	V_{on} (V)	0.51	0.58	0.67
	I_R (A)	7.3×10^{-6}	7.0×10^{-6}	5.1×10^{-6}
	n	1.23	1.35	1.51

IV. CONCLUSION

This study thoroughly investigates the impact of proton irradiation on the performance of lateral and quasi-vertical GaN SBDs. Systematic simulations and experimental analyses

reveal that quasi-vertical GaN SBDs exhibit better performance compared to lateral GaN SBDs under 200-keV proton irradiation. For quasi-vertical GaN SBDs, the forward current primarily depends on the doping concentration in the N-GaN layer. Since this doping concentration is relatively high compared to the concentration of irradiation-induced acceptor defects, the compensation effect is minimal, leading to only a slight decrease in the forward current. However, the increase in the reverse current is attributed to the presence of shallow donor defects at the Metal/GaN interface, which enhances the trap TAT effect, allowing more electrons to tunnel from the metal into the GaN. For lateral AlGaN/GaN SBDs, defects in the AlGaN layer become negatively charged when electrons are trapped, creating an inverse polarization field at the heterojunction surface. This reduces the polarization intensity and lowers the 2DEG concentration, which is the primary reason for forward current degradation in lateral diodes after irradiation. Additionally, the AlGaN layer prevents electrons from directly tunneling from the metal into the GaN, so shallow donor defects in the GaN channel layer do not contribute to the tunneling current. The decline in the reverse current is due to irradiation-induced acceptor defects in the GaN channel layer beneath the cathode, which traps electrons.

REFERENCES

[1] K. J. Chen et al., "GaN-on-Si power technology: Devices and applications," *IEEE Trans. Electron Devices*, vol. 64, no. 3, pp. 779–795, Mar. 2017.

[2] S. J. Pearton and F. Ren, "GaN electronics," *Adv. Mater.*, vol. 12, no. 21, pp. 1571–1580, Nov. 2000.

[3] R. Zhao et al., "Fast recovery performance and design method for high-power microwave limiter using GaN-SBD technology," *IEEE Trans. Microw. Theory Techn.*, vol. 72, no. 8, pp. 4822–4832, Aug. 2024.

[4] S. Han, S. Yang, R. Li, X. Wu, and K. Sheng, "Current-collapse-free and fast reverse recovery performance in vertical GaN-on-GaN Schottky barrier diode," *IEEE Trans. Power Electron.*, vol. 34, no. 6, pp. 5012–5018, Jun. 2019.

[5] Y. Zhang et al., "GaN-on-Si vertical Schottky and p-n diodes," *IEEE Electron Device Lett.*, vol. 35, no. 6, pp. 618–620, Jun. 2014.

[6] F. Zhou et al., "High-voltage quasi-vertical GaN junction barrier Schottky diode with fast switching characteristics," *IEEE Electron Device Lett.*, vol. 42, no. 7, pp. 974–977, Jul. 2021.

[7] M. Zhu et al., "1.9-kV AlGaN/GaN lateral Schottky barrier diodes on silicon," *IEEE Electron Device Lett.*, vol. 36, no. 4, pp. 375–377, Apr. 2015.

[8] E. Bahat-Treidel et al., "Fast-switching GaN-based lateral power Schottky barrier diodes with low onset voltage and strong reverse blocking," *IEEE Electron Device Lett.*, vol. 33, no. 3, pp. 357–359, Mar. 2012.

[9] S. Li et al., "Reliability concern of quasi-vertical GaN Schottky barrier diode under high temperature reverse bias stress," *Superlattices Microstruct.*, vol. 130, pp. 233–240, Jun. 2019.

[10] M. A. Khan, J. N. Kuznia, J. M. Van Hove, N. Pan, and J. Carter, "Observation of a two-dimensional electron gas in low pressure metalorganic chemical vapor deposited GaN-$Al_xGa_{1-x}N$ heterojunctions," *Appl. Phys. Lett.*, vol. 60, no. 24, pp. 3027–3029, Jun. 1992.

[11] M. A. Khan, A. Bhattarai, J. N. Kuznia, and D. T. Olson, "Observation of a two-dimensional electron gas in low pressure metalorganic chemical vapor deposited GaN-$Al_xGa_{1-x}N$ heterojunctions," *Appl. Phys. Lett.*, vol. 63, no. 9, pp. 1214–1215, Aug. 1993.

[12] D. M. Fleetwood, E. X. Zhang, R. D. Schrimpf, and S. T. Pantelides, "Radiation effects in AlGaN/GaN HEMTs," *IEEE Trans. Nucl. Sci.*, vol. 69, no. 5, pp. 1105–1119, May 2022.

[13] S. J. Pearton, F. Ren, E. Patrick, M. E. Law, and A. Y. Polyakov, "Review—Ionizing radiation damage effects on GaN devices," *ECS J. Solid State Sci. Technol.*, vol. 5, no. 2, pp. Q35–Q60, 2016.

[14] S. J. Pearton and R. Deist, "Review of radiation damage in GaN-based materials and devices," *J. Vac. Sci. Technol. A, Vac. Surf. Films*, vol. 31, no. 5, Jan. 2016, Art. no. 050801.

[15] M. P. King et al., "Performance and breakdown characteristics of irradiated vertical power GaN P-i-N diodes," *IEEE Trans. Nucl. Sci.*, vol. 62, no. 6, pp. 2912–2918, Dec. 2015.

[16] L. Lv et al., "Fast and thermal neutron radiation effects on GaN PIN diodes," *IEEE Trans. Nucl. Sci.*, vol. 64, no. 1, pp. 643–647, Jan. 2017.

[17] Z. Zhang et al., "Thermal stability of deep level defects induced by high energy proton irradiation in n-type GaN," *J. Appl. Phys.*, vol. 118, no. 15, Oct. 2015, Art. no. 155701.

[18] G. A. Umana-Membreno, J. M. Dell, G. Parish, B. D. Nener, L. Faraone, and U. K. Mishra, "^{60}Co gamma irradiation effects on n-GaN Schottky diodes," *IEEE Trans. Electron Devices.*, vol. 50, no. 12, pp. 2326–2334, Dec. 2003.

[19] A. P. Karmarkar et al., "Proton-induced damage in gallium nitride-based Schottky diodes," *IEEE Trans. Nucl. Sci.*, vol. 52, no. 6, pp. 2239–2244, Dec. 2005.

[20] X.-F. Zheng et al., "Characterization of bulk traps and interface states in AlGaN/GaN heterostructure under proton irradiation," *Appl. Phys. Lett.*, vol. 112, no. 23, Jun. 2018, Art. no. 233504.

[21] A. Y. Polyakov et al., "Effects of proton implantation on electrical and recombination properties of n-GaN," *Solid-State Electron.*, vol. 44, no. 11, pp. 1971–1983, Nov. 2000.

[22] C. G. Van de Walle and J. Neugebauer, "First-principles calculations for defects and impurities: Applications to III-nitrides," *J. Appl. Phys.*, vol. 95, no. 8, pp. 3851–3879, Mar. 2004.

[23] T. Mattila and R. M. Nieminen, "*Ab initio* study of oxygen point defects in GaAs, GaN, and AlN," *Phys. Rev. B, Condens. Matter*, vol. 54, no. 23, pp. 16676–16682, Dec. 1996.

[24] D. M. Fleetwood, X. Li, E. X. Zhang, R. D. Schrimpf, and S. T. Pantelides, "Low-frequency noise due to iron impurity centers in GaN-based HEMTs," *IEEE Trans. Electron Devices*, vol. 71, no. 2, pp. 1024–1030, Feb. 2024.

[25] D. Wickramaratne, J.-X. Shen, C. E. Dreyer, A. Alkauskas, and C. G. Van de Walle, "Electrical and optical properties of iron in GaN, AlN, and InN," *Phys. Rev. B, Condens. Matter*, vol. 99, no. 20, May 2019, Art. no. 205202.

[26] D. W. Cardwell et al., "Spatially-resolved spectroscopic measurements of E_c–0.57 eV traps in AlGaN/GaN high electron mobility transistors," *Appl. Phys. Lett.*, vol. 102, no. 19, May 2013, Art. no. 193509.

[27] M. Silvestri, M. J. Uren, and M. Kuball, "Iron-induced deep-level acceptor center in GaN/AlGaN high electron mobility transistors: Energy level and cross section," *Appl. Phys. Lett.*, vol. 102, no. 7, Feb. 2013, Art. no. 073501.

[28] K. H. Chow et al., "Intrinsic defects in GaN. I. Ga sublattice defects observed by optical detection of electron paramagnetic resonance," *Phys. Rev. B, Condens. Matter*, vol. 69, no. 4, Jan. 2004, Art. no. 045207.

[29] Y. S. Puzyrev, T. Roy, E. X. Zhang, D. M. Fleetwood, R. D. Schrimpf, and S. T. Pantelides, "Radiation-induced defect evolution and electrical degradation of AlGaN/GaN high-electron-mobility transistors," *IEEE Trans. Nucl. Sci.*, vol. 58, no. 6, pp. 2918–2924, Dec. 2011.

[30] J. V. Logan, K. B. Woller, P. T. Webster, C. P. Morath, and M. P. Short, "Open volume defect accumulation with irradiation in GaN, GaP, InAs, InP, Si, ZnO, and MgO," *J. Appl. Phys.*, vol. 134, no. 22, Dec. 2023, Art. no. 225701.

[31] C.-W. Wang, "Neutron irradiation effect on radio-frequency magnetron-sputtered GaN thin films and Au/GaN Schottky diodes," *J. Vac. Sci. Technol. B, Microelectron. Nanometer Struct. Process., Meas., Phenomena*, vol. 20, no. 5, pp. 1821–1826, Oct. 2002.

[32] T. Roy et al., "Temperature-dependence and microscopic origin of low frequency 1/f noise in GaN/AlGaN high electron mobility transistors," *Appl. Phys. Lett.*, vol. 99, no. 20, Nov. 2011, Art. no. 203501.

[33] M. D. McCluskey, N. M. Johnson, C. G. Van de Walle, D. P. Bour, M. Kneissl, and W. Walukiewicz, "Metastability of oxygen donors in AlGaN," *Phys. Rev. Lett.*, vol. 80, no. 18, pp. 4008–4011, May 1998.

[34] J. Joh and J. A. del Alamo, "Mechanisms for electrical degradation of GaN high-electron mobility transistors," in *IEDM Tech. Dig.*, San Francisco, CA, USA, Dec. 2006, pp. 1–4.

[35] B. D. White et al., "Electrical, spectral, and chemical properties of 1.8 MeV proton irradiated AlGaN/GaN HEMT structures as a function of proton fluence," *IEEE Trans. Nucl. Sci.*, vol. 50, no. 6, pp. 1934–1941, Dec. 2003.

[36] X. Li et al., "Defect and impurity-center activation and passivation in irradiated AlGaN/GaN HEMTs," *IEEE Trans. Nucl. Sci.*, vol. 71, no. 1, pp. 80–87, Jan. 2024.